1988

Electrodeposition of Copper-Nickel Alloys from Citrate Solutions on a Rotating Disk Electrode

Ramona Y. Ying

Patrick K. Ng

Z. Mao
Texas A & M University - College Station

Ralph E. White
University of South Carolina - Columbia, white@cec.sc.edu

Publication Info

Journal of the Electrochemical Society, 1988, pages 2964-2971.

DOI: 10.1149/1.2095470
http://dx.doi.org/10.1149/1.2095470

port conditions on the reaction surface and helped smooth the deposit at the expense of the current efficiency. As the hydrogen evolution reaction dominates over 90% of the process, the alloy deposit loses its integrity. Note in Fig. 14g for the Cu-5 bath at −1.6V, segregated areas of copper-rich and nickel-rich can be seen as well as numerous cracks caused by hydrogen embrittlement.

Conclusions

Codeposition of copper-nickel alloys occurs in a fairly narrow potential region, namely, between −1.0 to −1.2V *vs.* SCE. In this region, a wide variety of alloy composition (0-50% nickel) and fairly smooth deposits can be obtained. Because copper deposition is near mass transport limited in the codeposition region, it is important that the plating bath is well-agitated. The composition of the alloy deposit can be controlled by the molar metal ion ratio in solution as well as the electrode potential. If greater operational control is needed, alternative plating schemes such as pulse plating can be utilized. Preliminary pulse-potential deposition of this alloy produced some improved surface morphology as well as greater compositional control. Also, for greater applicability, it is useful to model the alloy deposition process as discussed in part II of this paper (18).

Acknowledgments

The author wishes to thank Robert F. Paluch for the EDX/SEM work and Audry A. Dow for the Auger electron spectroscopy analysis. Also, the insightful comments of S. Swathirajan are greatly appreciated.

Manuscript submitted Dec. 14, 1987; revised manuscript received May 2, 1988.

General Motors Research Laboratories assisted in meeting the publication costs of this article.

REFERENCES

1. C. Kato and H. W. Pickering, *This Journal*, **131,** 1219 (1984).
2. H. P. Dhar, R. E. White, G. Burnell, L. E. Cornwell, R. B. Griffin, and R. Darby, *Corrosion NACE*, **41,** 317 (June 1985).
3. P. K. Chauhan and H. S. Gadiyar. *Corros. Sci.*, **25,** 55 (1985).
4. W. Z. Friend, "Corrosion of Nickel and Nickel Base Alloy," pp. 95-135, Wiley-Interscience Publication, New York (1980).
5. J. H. Sinfelt, "Bimetallic Catalysts," pp. 20-31, John Wiley & Sons, Inc., New York (1983).
6. G. Bruni and M. Amadori, *Atti e mem. regia acad. sci., lettere ed arti Padova,* **28,** Part IV, p. 181 (1912).
7. A. Brenner, "Electrodeposition of Alloys," Vol. 1, pp. 559-584, Academic Press, Inc., New York (1963).
8. H. D. Hineline and W. B. Cooley, *Trans. Am. Electrochem. Soc.*, **48,** 61 (1925).
9. P. Silvestroni and G. A. Sartori, *Ricerca Sci.*, **17,** 1156 (1957).
10. L. E. Stout and C. L. Faust, *Trans. Electrochem. Soc.*, **60,** 271 (1931).
11. B. H. Priscott, *Trans. Inst. Met. Finish.*, **36,** 93 (1959).
12. J. R. Roos, J. P. Celis, C. Buelens, and D. Goris, *Proc. Metall.*, **3,** 177 (1984).
13. K. Vu Quang, E. Chassaing, B. Le Viet, J. P. Celis, and J. R. Roos, *Met. Finish.*, 25 (Oct. 1985).
14. N. Ya Gavrilova and A. M. Ozerov, *Prot. Met.*, **8,** 310 (1972).
15. M. Ishikawa and H. Enomoto, "New Materials & New Processes," **2,** pp. 243-251 (1983).
16. Y. N. Sadana and T. K. Venkatachalam, *Met. Finish.*, 15 (Aug. 1979).
17. Y. N. Sadana, A. K. Despande, and R. N. Gedye, *Surf. Tech.*, **17,** 111 (1982).
18. R. Y. Ying, P. K. Ng, Z. Mao, and R. E. White, *This Journal*, **135,** 2964 (1988).
19. S. Swathirajan and S. Bruckenstein, *Z. Phys. Chem.*, **136,** 215 (1983).
20. T. I. Quickenden and X. Jiang, *Electrochim Acta*, **29,** 693 (1984).
21. R. Y. Ying, R. Moy, L. C. Fraser, B. S. O'Bannion, and F. M. Donahue, *This Journal*, **135,** 654 (1988).
22. A. Knoedler, Ch. J. Raub, and E. Raub, *Metalloberflaeche Agnew Elektrochem.*, **38,** 496 (1984).
23. E. Chassaing, K. Vu Quang, and R. Wiart, *J. Appl. Electrochem.*, **16,** 591 (1986).
24. A Saraby-Reintjes and M. Fleischmann, *Electrochim. Acta*, **29,** 557 (1984).

Electrodeposition of Copper-Nickel Alloys from Citrate Solutions on a Rotating Disk Electrode

II. Mathematical Modeling

Ramona Y. Ying* and Patrick K. Ng*,[1]

General Motors Research Laboratories, Physical Chemistry Department, Warren Michigan 48090-9055

Z. Mao and Ralph E. White*

Department of Chemical Engineering, Texas A&M University, College Station, Texas 77843-3122

ABSTRACT

A mathematical model is developed to simulate the electrodeposition of Cu-Ni alloy from citrate solutions onto a rotating disk electrode under potentiostatic control. The model includes the influence of diffusion, ionic migration, forced convection, and homogeneous equilibria. The three major electrochemical reactions treated in the model are copper deposition, nickel deposition, and hydrogen evolution. Using experimental parameters when available, the model was fitted and tested against experimentally-obtained results for different bath compositions and operating conditions. The model agreed reasonably well with the experimental results particularly in the codeposition region, −1.0 to −1.2V *vs.* SCE, where hydrogen evolution is not the major reaction. Also, the model's predictive capabilities are evaluated.

Electrodeposition of copper-nickel alloys has potential industrial applications due to the alloy's resemblance to Monel alloy, which is widely used in marine installation. For instance, the corrosion current densities of a 20-30% copper alloy coating in a 3% NaCl solution have been measured to be between 0.3 and 0.6 $\mu A/cm^2$, which are similar to the corrosion rate of Monel 400 (1). Thus, a sound, coherent Cu-Ni alloy deposit can be used as a protective coating against such salt environment. Other attractive features, besides corrosion resistance, include malleability, ductility, and solderability.

* Electrochemical Society Active Member.
[1] Present address: Digital Equipment Corporation, Colorado Springs, Colorado 80907.

The Cu-Ni alloy plating process is classified as a normal alloy deposition type since the more noble metal, copper in this case, deposits preferentially (2). Very often a complexing agent is needed to codeposit the metals. Over the years, many complex agents have been tried; the consensus is that citrate and pyrophosphate are the most promising ones (1-5). As with most normal type of alloy deposition, the conditions needed to plate a high-nickel alloy deposit are a much higher ratio of nickel-to-copper in solution as well as a large applied current density. Other important parameters include the *p*H, agitation, and temperature. Priscott (3) found that the cathode current efficiency dropped as the *p*H was lowered. Also, he showed that the copper content in the alloy deposit increased slightly with agitation. These parameters, namely, solution composition, deposition potential (or current), *p*H, and agitation, will be examined further in our report. However, the effect of temperature was negligible (3) and was not studied.

Commercially useful alloys in terms of deposit composition, morphology, and adhesion are difficult to obtain. There appears to be a narrow range of suitable operating conditions for a sound, coherent deposit. Otherwise the deposit can be dark, "burnt," and powdery. Most studies (1-5) related the deposit composition as a function of the applied current density, which is strongly dependent on the solution composition. Unfortunately, the solution compositions varied so widely that it is difficult to draw useful information from such studies.

We found the need to understand the fundamental aspects involved in the Cu-Ni alloy plating process as well as to model the system for general application. The previous report (6) dealt with the former topic. In that paper (6), five electrochemical reactions were identified to occur during Cu-Ni alloy electrodeposition. Copper and nickel codeposit in a narrow potential region, −1.0 to −1.2V *vs.* SCE, where the effects of the other three electrode reactions are small. Some of the mass transport and kinetic parameters for the codeposition process were determined. Also, the alloy deposits were plated at constant potentials and characterized. The electrode potential instead of the current density was chosen as the operating variable for convenience.

In the present report, a mathematical model is developed to describe the codeposition of copper and nickel in a citrate solution. The model takes into account factors affecting the transport of species in solution such as diffusion, migration, and forced convection. In addition, the homogeneous chemical equilibria among the species in the plating solution are also considered. The model was tested against the experimental results from our previous work (6) and was also used for predicting the optimum plating conditions.

Recently, Mathias and Chapman (7) applied a similar model to the Zn-Ni alloy system. They were able to predict the alloy composition fairly well; however, the disagreement between the model prediction and the polarization data demonstrated that their kinetic model was inappropriate in describing the anomalous behavior of Zn-Ni alloy plating. However, the Cu-Ni system behaves more ideally such that its codeposition is classified as normal and that it exhibits a continuous series of homogeneous solid solutions.

Equilibrium Bulk Conditions

In modeling the alloy deposition process, it is essential to know the bulk and surface concentrations of the reactants in order to assess the magnitude of the mass-transfer effects and reaction rates. As mentioned earlier, the copper-nickel alloy plating bath typically requires a complexing agent to codeposit the metals. Citrate, one of the most promising ligands for the Cu-Ni alloy system, is used in the present study. The bulk concentrations are calculated by using the equilibrium constants, material conservation equations, and the electroneutrality condition. According to the literature (8-10) in a bath containing copper sulfate ($CuSO_4 \cdot 5H_2O$), nickel sulfate ($NiSO_4 \cdot 6H_2O$), and sodium citrate ($Na_3C_6H_5O_7 \cdot 2H_2O$), the following equilibria are possible

$$Cu^{2+} + Cit^{3-} \rightleftharpoons CuCit^- \quad [1]$$

$$Cu^{2+} + HCit^{2-} \rightleftharpoons CuHCit \quad [2]$$

$$HCit^{2-} \rightleftharpoons H^+ + Cit^{3-} \quad [3]$$

$$H_2Cit^- \rightleftharpoons H^+ + HCit^{2-} \quad [4]$$

$$H_3Cit \rightleftharpoons H^+ + H_2Cit^- \quad [5]$$

$$Ni^{2+} + Cit^{3-} \rightleftharpoons NiCit^- \quad [6]$$

$$Ni^{2+} + HCit^{2-} \rightleftharpoons NiHCit \quad [7]$$

$$SO_4^{2-} + H^+ \rightleftharpoons HSO_4^- \quad [8]$$

$$H_2O \rightleftharpoons OH^- + H^+ \quad [9]$$

where Cit^{3-} is $C_6H_5O_7^{3-}$. The material balances for the species in Eq. [1]-[9] are

$$[Cu^{2+}]_{total} = [Cu^{2+}] + [CuCit^-] + [CuHCit] \quad [10]$$

$$[Ni^{2+}]_{total} = [Ni^{2+}] + [NiCit^-] + [NiHCit] \quad [11]$$

$$[Cit^{3-}]_{total} = [Cit^{3-}] + [CuCit^-] + [CuHCit] + [NiCit^-] + [NiHCit] + [HCit^{2-}] + [H_2Cit^-] + [H_3Cit] \quad [12]$$

$$[SO_4^{2-}]_{total} = [SO_4^{2-}] + [HSO_4^-] \quad [13]$$

where $[i]_{total}$ is the concentration of species i added to the bulk solution. The electroneutrality condition is

$$\sum_i z_i c_i = 0 \quad [14]$$

The equilibrium constants for Eq. [1]-[9] are listed in Table I. The algorithm for the equilibrium calculation is outlined in the Appendix. Basically, the program uses the experimentally measured *p*H and the initial species concentrations, $[i]_{total}$, to calculate the equilibrium concentrations of all species. The computed results are given in Table II for the three plating solutions: Cu-5, Cu-10, and Cu-20 baths, which are labeled according to the percentage of cupric ion in the solutions containing 0.19*M* total metal ion concentration. The measured *p*H values for these baths are 5.37, 5.06, and 4.76, respectively.

In order to satisfy electroneutrality, a pseudo species was conceived to allow for any unknown species in the so-

Table I. Equilibrium constants

Reaction j	Constant	Reference
1	1.58×10^{14} liter/mol	Lange (8)
2	2.22×10^{4} liter/mol	Lange (8)
3	4.02×10^{-7} mol/liter	CRC (9)
4	1.75×10^{-5} mol/liter	CRC (9)
5	7.43×10^{-4} mol/liter	CRC (9)
6	1.99×10^{14} liter/mol	Lange (8)
7	1.29×10^{5} liter/mol	Lange (8)
8	8.33×10^{1} liter/mol	CRC (9)
9	1.00×10^{-14} (mol/liter)^2	CRC (9)

Table II. Concentrations for the three plating baths

Bath Species i	Cu-5[a] $c_{i,\infty}$(mol/liter)	Cu-10[b] $c_{i,\infty}$(mol/liter)	Cu-20[c] $c_{i,\infty}$(mol/liter)
$CuCit^-$	0.9500×10^{-2}	0.1900×10^{-1}	0.3800×10^{-1}
CuHCit	0.1416×10^{-10}	0.5781×10^{-10}	0.2307×10^{-9}
Cu^{2+}	0.1312×10^{-13}	0.6200×10^{-13}	0.3256×10^{-12}
Cit^{3-}	0.4573×10^{-2}	0.1936×10^{-2}	0.7373×10^{-3}
$HCit^{2-}$	0.4853×10^{-1}	0.4194×10^{-1}	0.3187×10^{-1}
H_2Cit^-	0.1183×10^{-1}	0.2088×10^{-1}	0.3165×10^{-1}
H_3Cit	0.6792×10^{-4}	0.2447×10^{-3}	0.7402×10^{-3}
$NiCit^-$	0.1805×10^{0}	0.1710×10^{0}	0.1520×10^{0}
NiHCit	0.1242×10^{-8}	0.2402×10^{-8}	0.4259×10^{-8}
Ni^{2+}	0.1983×10^{-12}	0.4439×10^{-12}	0.1036×10^{-11}
SO_4^{2}	0.1899×10^{0}	0.1899×10^{0}	0.1897×10^{0}
HSO_4^-	0.6749×10^{-4}	0.1377×10^{-3}	0.2746×10^{-3}
H^+	0.4266×10^{-5}	0.8710×10^{-5}	0.1738×10^{-4}
OH^-	0.2344×10^{-8}	0.1148×10^{-8}	0.5754×10^{-9}
Na^+	0.7650×10^{0}	0.7650×10^{0}	0.7650×10^{0}
Pseudo$^-$	0.7246×10^{-1}	0.8458×10^{-1}	0.9769×10^{-1}

[a] Cu-5: $[CuSO_4] = 0.0095M$, $[NiSO_4] = 0.1805M$, $[Na_3Cit] = 0.255M$
[b] Cu-10: $[CuSO_4] = 0.019M$, $[NiSO_4] = 0.171M$, $[Na_3Cit] = 0.255M$
[c] Cu-20: $[CuSO_4] = 0.038M$, $[NiSO_4] = 0.152M$, $[Na_3Cit] = 0.255M$

lutions. Usually, the pH of the deionized water was found to be less than 7, suggesting that some unknown anions were omitted in the calculations. Other examples of pseudo species are carbonates or metal salt impurities assayed in the reagent grade chemicals.

As shown in Table II, the major reactant species in the bulk solution are the metal complexes $CuCit^-$ and $NiCit^-$. In comparison, the concentrations of the other metal species (CuHCit, Cu^{2+}, NiHCit, and Ni^{2+}) are small. Consequently, the reductions of these species at the electrode surface are neglected in the model. Thus, the homogeneous equilibria, Eq. [1] and [6] are included in the model. Also, only the first hydrogenation of the citrate ion, *i.e.*, Eq. [3], is considered. Finally, since hydrogen evolution from the reduction of water plays a significant role in the alloy deposition, the water equilibrium, Eq. [9], is also incorporated in the model. Hence, only four homogeneous equilibria [1], [3], [6], and [9]) are included in the model for the diffusion layer.

The pH of the plating bath can be adjusted by adding sulfuric acid or sodium hydroxide. The predicted effect of the pH on the metal species concentrations is shown in Fig. 1. The figure indicates that unless the pH is fairly low (*i.e.*, less than 3), the predominant metal species are complexed with citrate ion. Thus, the above assumptions should be valid for solutions whose pH is above 3, but less than about 8 due to possible nickel hydroxide formation. As will be discussed later, it is not desirable to operate at low pH because of the loss in current efficiency, which is affected by the magnitude of the hydrogen evolution reaction.

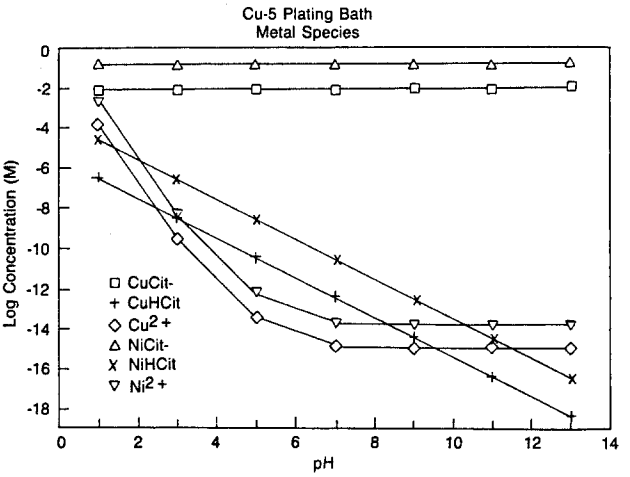

Fig. 1. The dependence of the cupric and nickel ion species on pH in the Cu-5 plating bath: $[CuSO_4] = 0.0095M$, $[NiSO_4] = 0.1805M$, and $[Na_3Cit] = 0.255M$.

Mathematical Model

The model presented here was established to simulate the characteristics of the electrodeposition for steady state at a constant potential difference between the working electrode and a reference electrode in the bulk solution. In the model, the infinite dilute solution theory was assumed, and the current density took the form of the Butler-Volmer equation. The solid phase was approximated by an ideal solid solution such that no interaction between copper and nickel was assumed.

At steady state, the region outside the electrode surface is governed by the following mass balance equation for each species

$$-\nabla \cdot N_i + R_i = 0 \qquad [15]$$

where R_i is the production of the species i in solution, and is zero for inert species such as Na^+ and SO_4^{2-}. The flux, N_i, includes the effects of convective diffusion, forced convection, and ionic migration. For the rotating disk system, Eq. [15] can be written in dimensionless form as (11)

$$\frac{D_i}{D_R}\frac{d^2c_i}{d\xi^2} + 3\xi^2\frac{dc_i}{d\xi} + \frac{z_iD_i\mathbf{F}}{RT\cdot D_R}\left[c_i\frac{d^2\Phi}{d\xi^2} + \frac{dc_i}{d\xi}\frac{d\Phi}{d\xi}\right] + \frac{\delta^2}{D_R}R_i = 0$$

$$i = 1, 2, \ldots, n \qquad [16]$$

where $\xi = y/\delta$ is a dimensionless normal distance from the surface of the electrode into the electrolyte, Φ is the potential in the solution, and δ is the Levich diffusion layer thickness given by

$$\delta = \left(\frac{3D_R}{a\nu}\right)^{1/3}\left(\frac{\nu}{\omega}\right)^{1/2} \qquad [17]$$

Equation [16] provides a set of n equations with $n + 1$ unknowns (c_i for $i = 1$ to n and Φ). To make this set of equations solvable, another equation is needed. The electroneutrality condition can be used for this purpose

$$\sum_i z_ic_i = 0 \qquad [18]$$

The species included in the model for the diffusion layer and electrode surface are: Cu^{2+}, Cit^{3-}, $CuCit^-$, Ni^{2+}, $NiCit^-$, H^+, OH^-, $HCit^{2-}$, SO_4^{2-}, and Na^+.

To simplify the calculation, the homogeneous chemical reactions (Eq. [1], [3], [6], and [9]) included in the diffusion layer are assumed to be kinetically much faster than the heterogeneous surface electrode reactions, so R_i can be eliminated from Eq. [15]. For example, from Eq. [1], one can write the following equation

$$R_{Cu^{2+}} = -R_{CuCit^-} \qquad [19]$$

With this equation, the two governing equations (Eq. [15]) for Cu^{2+} and $CuCit^-$ can be combined to give

$$\nabla \cdot N_{Cu^{2+}} + \nabla \cdot N_{CuCit^-} = 0 \qquad [20]$$

and the concentration of citrate is then given by

$$K_1 = \frac{C_{CuCit^-}}{C_{Cu^{2+}}\cdot C_{Cit^{3-}}} \qquad [21]$$

where K_1 is the equilibrium constant for Eq. [1]. The complete set of governing equations is shown in Table III.

The boundary conditions for the model consist of those at the electrode surface and those in the bulk solution. At the electrode surface, the following reactions are assumed to occur

$$CuCit^- + 2e^- \rightarrow Cu + Cit^{-3} \qquad [22]$$

$$NiCit^- + 2e^- \rightarrow Ni + Cit^{-3} \qquad [23]$$

and

$$2H_2O + 2e^- \rightarrow H_2 + 2\,OH^- \qquad [24]$$

Two of the five electrochemical reactions found to occur during Cu-Ni alloy plating (6) are ignored. They are the reduction of hydrogen ion from the dissociation of hydrogenated citrate ions and the reduction of dissolved oxygen. The former reaction is assumed to be small compared to the reduction of water at large negative potentials where codeposition occurs. The latter reaction is completely mass transport limited and its effect is combined with the copper deposition reaction. In other words, the mass transport and kinetic parameters determined for the copper deposition reaction were based on the polarization data taken in an aerated solution where the effects of oxygen reduction are included (6).

Table III. Governing equations

1.	$\nabla \cdot N_{Cu^{2+}} + \nabla \cdot N_{CuCit^-} = 0$
2.	$\nabla \cdot N_{Ni^{2+}} + \nabla \cdot N_{NiCit^-} = 0$
3.	$\nabla \cdot N_{Cit^{3-}} + \nabla \cdot N_{CuCit^-} + \nabla \cdot N_{NiCit^-} + \nabla \cdot N_{HCit^{2-}} = 0$
4.	$\nabla \cdot N_{H^+} + \nabla \cdot N_{HCit^{2-}} - \nabla \cdot N_{OH^-} = 0$
5.	$K_1 = C_{CuCit^-}/\{C_{Cu^{2+}} \cdot C_{Cit^{3-}}\}$
6.	$(K_3)^{-1} = C_{HCit^{2-}}/\{C_{H^+} \cdot C_{Cit^{3-}}\}$
7.	$K_6 = C_{NiCit^-}/\{C_{Ni^{2+}} \cdot C_{Cit^{3-}}\}$
8.	$K_9 = C_{H^+} \cdot C_{OH^-}$
9.	$\nabla \cdot N_{SO_4^{2-}} = 0$
10.	$\nabla \cdot N_{Na^+} = 0$
11.	$\sum_i z_ic_i = 0$

The flux of each species equals the amount of the species consumed by the electrode reactions

at $\xi = 0$

$$N_i + \sum_{j=1}^{m} \frac{s_{ij} i_j}{n_j \mathbf{F}} = 0 \quad [25]$$

where

$$N_i = -\frac{D_i}{\delta}\frac{dc_i}{d\xi} - \frac{z_i D_i c_i \mathbf{F}}{RT \cdot \delta}\frac{d\Phi}{d\xi} \quad [26]$$

$$i_j = i_{oj,ref}\left\{\left[\prod_i \left(\frac{c_{i,o}}{c_{i,ref}}\right)^{P_{ij}}\right]\left(\prod_k a_k^{\gamma_{kj}}\right)\exp\left[\frac{\alpha_{aj}\mathbf{F}}{RT}\left(V - \Phi_{RE} - \left[\Phi_o - \Phi_{RE}\right] - U_{j,ref}\right)\right] - \left[\prod_i \left(\frac{c_{i,o}}{c_{i,ref}}\right)^{q_{ij}}\right]\exp\left(\frac{-\alpha_{cj}\mathbf{F}}{RT}\left[V - \Phi_{RE} - (\Phi_o - \Phi_{RE}) - U_{j,ref}\right]\right)\right\} \quad [27]$$

and s_{ij} is the stoichiometric coefficient of species i in reaction j, i_j is the current density due to electrode reaction j, $U_{j,ref}$ is the theoretical open-circuit potential evaluated at reference concentrations (usually the bulk concentrations), and V is a potential of the working electrode. The relative activity of each metal, a_k, is taken to be equal to its mole fraction in the deposit, χ_k. The meanings of the other terms in Eq. [27] are given in the notation list and are discussed in Ref. (12). Two additional equations are required to describe the alloy composition

$$\chi_{Ni} = \frac{i_{Ni}}{i_{Ni} + i_{Cu}} \quad [28]$$

and

$$\chi_{Ni} + \chi_{Cu} = 1 \quad [29]$$

The electroneutrality condition is also applied because the diffuse double layer is ignored in the model.

Generally, beyond the distance of about two Levich diffusion layer thicknesses from the electrode, the concentrations of species can be considered to be equal to their bulk concentrations (13). In this system, the boundary conditions in the bulk solution is set at three diffusion layer thicknesses

at $\xi = 3$

$$c_i = c_{i,\infty} \quad [30]$$

$$\Phi = \Phi_{RE} \quad [31]$$

The bulk concentrations for the species considered in the model are presented in Table IV together with their diffusion coefficients. The concentrations of the neglected, ionic species (H_2Cit^-, HSO_4^-, and the pseudo species) from Table II were used to adjust the concentration of Na^+ in Table IV in order to sustain electroneutrality in the bulk solution. The set of governing equations and boundary conditions were written in finite difference form and solved by a technique developed by Newman (11, 14).

Table IV. Transport properties

Species i	D_i (cm²/s)	$c_{i,\infty}$ (mole/cm³)
Cu^{2+}	1.00×10^{-5}	0.1312×10^{-16}
Cit^{3-}	0.80×10^{-5}	0.4573×10^{-5}
$CuCit^-$	2.10×10^{-6}[a]	0.9500×10^{-5}
Ni^{2+}	1.00×10^{-5}	0.1983×10^{-15}
$NiCit^-$	0.25×10^{-7}[b]	0.1805×10^{-3}
H^+	1.00×10^{-4}	0.4266×10^{-8}
$HCit^{2-}$	0.73×10^{-5}	0.4853×10^{-4}
OH^-	5.50×10^{-5}	0.2344×10^{-11}
SO_4^{2-}	1.00×10^{-5}	0.1899×10^{-3}
Na^+	1.34×10^{-5}	0.6806×10^{-3}

[a] Experimental value.
[b] D_{NiCit}, based on model-experimental fit of the cathodic polarization curve at rotation speed 167.6 s^{-1} in the Cu-10 plating bath.

Table V. Kinetic parameters for electrode reactions

Reaction j	α_{cj}	n_j	$i_{oj,ref}$ (A/cm²)	U_j^a (V)
[22]	0.084[a]	2	2.6×10^{-3}[a]	−0.083
[23]	0.45[a]	2	1.0×10^{-4}[b]	−0.671
[24]	0.25	2	5.0×10^{-7}[b]	−0.828

[a] Experimental values.
[b] Based on model-experimental fit of the cathodic polarization curve at rotation speed 167.6 s^{-1} in the Cu-10 plating bath.

Model—Experimental Fit

To simulate accurately the experimental results, the basic kinetic and mass transport parameters are needed, preferably measured. In the previous report (6), some of these parameters were determined for the Cu-Ni alloy deposition process in citrate solutions on the rotating disk electrode. The experiments were performed at room temperature, and the kinetic data measured at a constant rotation speed, 1600 rpm (167.6 s^{-1}). For the copper deposition reaction (Eq. [22]), sufficient data were available to determine its kinetic parameters, such as the exchange current density and Tafel slope, as well as the diffusion coefficient of the complex containing copper. The kinetic parameters for the copper deposition reaction as well as for the other two reactions (Ni and H_2) are listed in Table V.

For the nickel deposition and hydrogen evolution reactions, the analysis was complicated by the fact that multiple reactions were occurring on the electrode surface. Consequently, the kinetic and mass-transfer parameters for these two reactions were difficult to determine accurately. Approximate magnitudes of these parameters, however, could be inferred by force fitting the model to one set of experimental data. As shown in Fig. 2, the model was first fitted for the Cu-10 bath between −0.5 to −1.3V. Above −0.5V, the main electrochemical reactions are the reductions of hydrogen ion from the dissociation of hydrogenated citrate ions and dissolved oxygen, which the model does not consider since it is mainly concerned with the codeposition region, −1.0 to −1.2V. From −0.5 to −1.0V, the copper deposition reaction dominates, so the fit in this region reflects the validity of the model in describing the copper reaction. At −1.0V, the effect of nickel deposition on the potential-current curve begins to appear. The codeposition region is very narrow because a substantial amount of hydrogen evolves at potentials more negative than −1.2V.

A valid test of the model is to use the same kinetic and mass transport parameters to fit the polarization data ob-

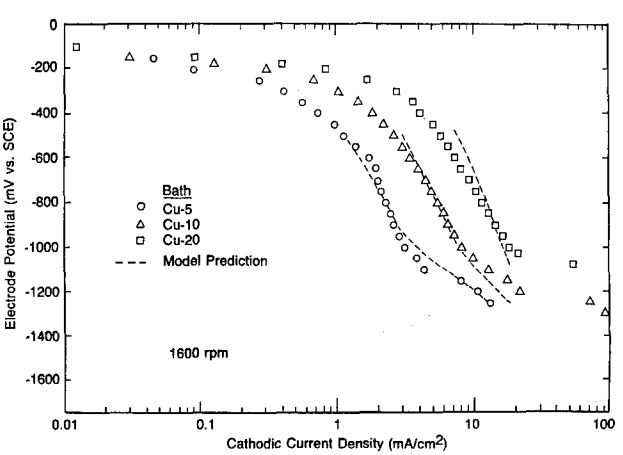

Fig. 2. Model-experimental fits of the cathodic polarization curves at different metal ratio in the alloy plating baths: total metal content = 0.19M and [Na_3Cit] = 0.255M. Rotation speed = 167.6 s^{-1}. Room temperature = 22°C.

tained at different operating conditions such as in the Cu-5 and Cu-20 baths (also shown in Fig. 2). For changes in solution composition, the exchange current density for copper deposition is dependent on the cupric ion concentration to the order of 1.43 according to the previous study (6). A first-order dependency on the nickel ion concentration is assumed for nickel deposition. A lower exchange current density for the hydrogen evolution reaction is used for the Cu-20 bath (2×10^{-7} mA/cm^2) because the alloy deposit has a higher copper content (6). As will be shown later, a better fit of the current efficiency data also resulted.

For all three plating baths, the model predictions agree reasonably well with the polarization data. Thus the adjustable parameters are fairly dependable. Consequently, the model can be used to estimate mass transport and kinetic parameters when multiple reactions are occurring simultaneously.

For the higher copper concentration baths (Cu-10 and Cu-20), a deviation from the data is observed at high negative potentials. The presence of the hydrogen bubbles at these potentials may have enhanced the mass transport conditions at the electrode surface, so that higher currents are measured. Experimentally, the currents are unsteady and continually increase with time under these conditions. It is beyond the scope of the model to treat such fluctuating processes.

The model can also be used to predict the alloy deposit compositions based upon the partial currents (Eq. [28] and [29]). Figure 3 depicts the model predictions of the alloy compositions (dashed lines) and the experimental values (symbols) as a function of deposition potential. The agreements are good in the potential region, −1.0 to −1.2V *vs.* SCE, where the influence of the hydrogen bubbles is small. Practically, this is the codeposition region of interest. Here, the current efficiency is sufficiently high and the surface morphology is relatively smooth, *i.e.*, not dendritic or powdery (6).

At more negative potentials, the model can be used to predict the leveling of the nickel content in the alloy deposit. The presence of hydrogen gas may have inhibited the diffusion of the nickel complex to the electrode possibly due to the concurrent hydrogen chemisorption and bubble formation. This is manifested by the low diffusion coefficient (0.25×10^{-7} cm^2/s) fitted for the nickel complex. When hydrogen evolution becomes dominant, however, the model fails to predict the drop in nickel content. The added forced convection produced by the gas bubbles, not considered in the model, may have enhanced the mass transport of copper ions and caused an increase in the copper content in the alloy deposits.

The deposit composition plot can be easily translated from being a function of deposition potential to a function of applied current density, with which most platers are familiar. From the polarization curves, the corresponding current density can be found for each deposition potential. In the deposition region of interest, −1.0 to −1.2V *vs.* SCE, the currents were fairly steady.

Figure 4 compares the experimental current efficiency data with that predicted by the model. The current efficiency is mostly influenced by the interference of the hydrogen evolution reaction during codeposition. For the Cu-5 and Cu-10 baths, the model predictions agree with the general dependence of the current efficiency with increasing negative potential. The agreement is not as good for the Cu-20 bath. As mentioned earlier, in the Cu-20 bath where the deposits are more copper-rich, the exchange current density for the reduction of water is assumed to be lower. This assumption is reasonable based upon the difference in the exchange current densities for hydrogen evolution on pure copper and pure nickel.

Between −1.0 to −1.1V, the model prediction of the current efficiency is about 5 to 10% higher than the experimental data. This deviation may be due to the added hydrogen evolution from the reduction of hydrogen ion from the dissociated hydrogenated citrate ions, which is not considered in the model. Also, the oxygen reduction reaction may also contribute to the lower current efficiency observed. At higher negative potentials, however, the reduction of water is the major contributor of hydrogen formation, and the model predictions are consistent.

In summary, the agreement between the model and experimental results is fairly good, demonstrating the validity of the model. The model was capable of predicting the polarization data, alloy composition, and current efficiency particularly in the codeposition region of interest, −1.0 to −1.2V. The model, however, does not account for all the consequences of the hydrogen evolution reaction. Although the model included its kinetics, it does not consider such effects as bubble nucleation, coalescence, and evolution, which can affect the mass transport conditions at the electrode surface. However, in a practical plating operation, hydrogen evolution should be avoided because of its detrimental effects on the surface morphology and current efficiency. Therefore, this model limitation is not too critical for designing or optimizing the plating conditions, but should be borne in mind. Nor does the model treat the second source of hydrogen evolution from the reduction of hydrogen ions from the dissociation of the hydrogenated citrate ions. This negligence causes the predicted current efficiency to be 5 to 10% higher than the measured result.

Model Predictions

One goal of modeling the Cu-Ni alloy deposition is to be able to predict the plating behavior for some yet-to-be

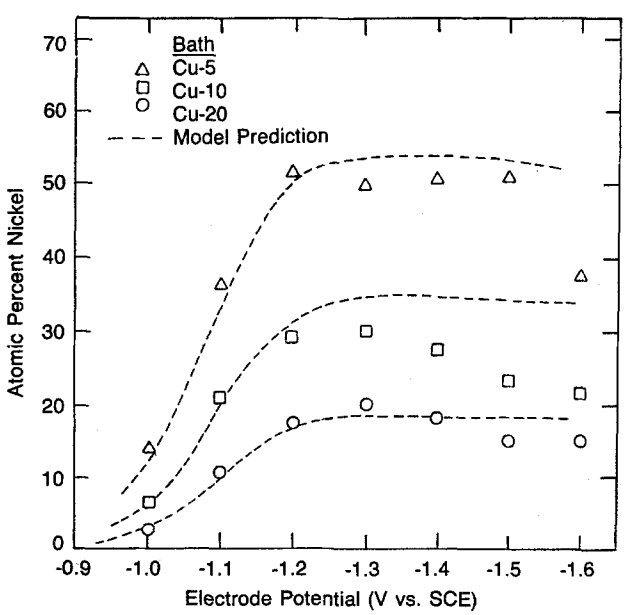

Fig. 3. Model-experimental fits of the alloy deposit composition as a function of deposition potential for three plating solutions: Cu-5, Cu-10, and Cu-20 baths. Rotation speed = 167.6 s^{-1}. Room temperature = 22°C.

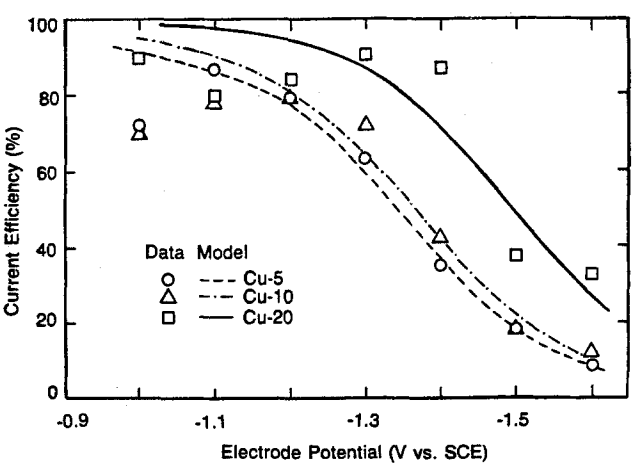

Fig. 4. Model-experimental fits of the current efficiency as a function of deposition potential for the three plating solutions: Cu-5, Cu-10, and Cu-20 baths. Rotation speed = 167.6 s^{-1}. Room temperature = 22°C.

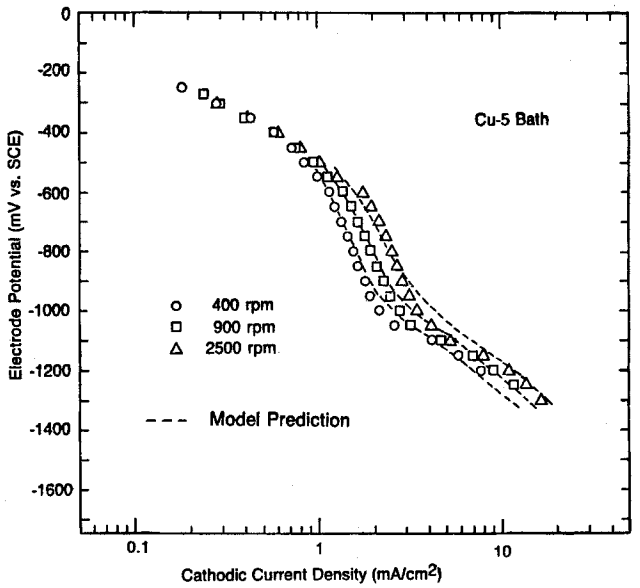

Fig. 5. Model-experimental fits of the cathodic polarization curves at different rotation speeds in the Cu-5 plating baths. Room temperature = 22°C.

measured operating conditions. Another goal may be to ascertain the operating conditions necessary to obtain a desired deposit composition. An example of each will be given. One important variable is the effect of stirring. Figures 5 and 6 illustrate the effect of rotation speed on the potential-current curves and deposit composition, respectively. From the previous report (6), polarization curves were measured as a function of rotation speed. Again, there is good agreement. Unfortunately, the deposit compositions were not measured. But based on Fig. 6, the rotation speed has a slight influence on the deposit composition. This result concurs with Priscott's findings (3). The amount of nickel in the deposit increases with lower rotation speeds. The more important variables in determining the deposit composition seem to be the solution composition and deposition potential. However, agitation is important in terms of the mass transport of the reactants to the electrode surface, thereby increasing the plating rate.

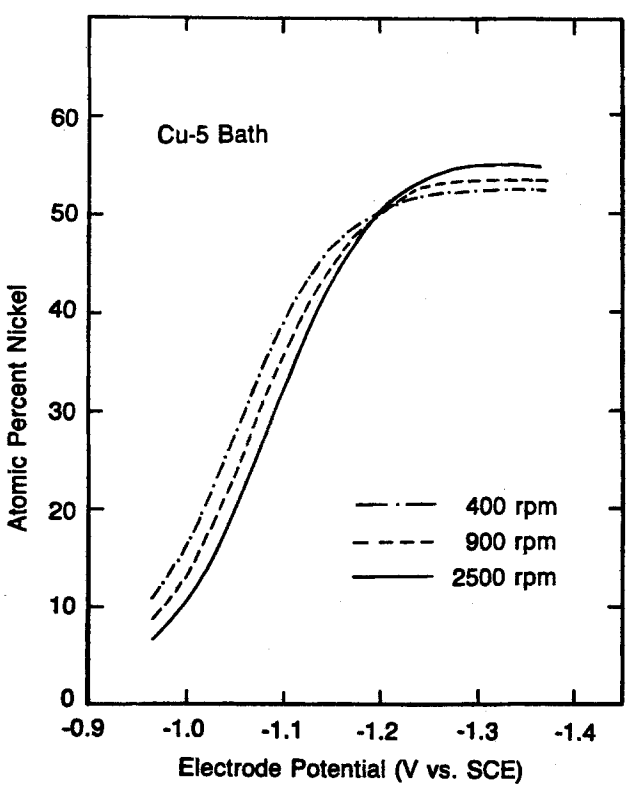

Fig. 6. Model prediction of the alloy deposit composition as a function of deposition potential at different rotation speeds in the Cu-5 plating bath. Room temperature = 22°C.

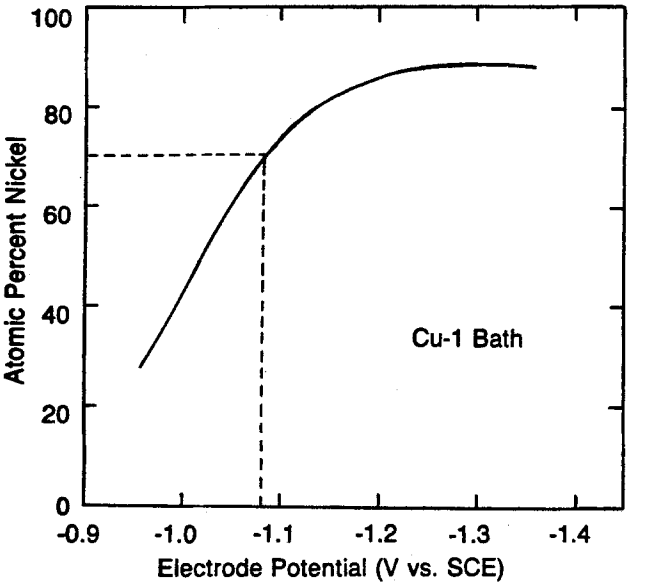

Fig. 7. Model prediction of the alloy deposit composition as a function of deposition potential in a plating bath containing 1% cupric ions: 0.0019M $CuSO_4$, 0.1881M $NiSO_4$, 0.255M Na_3Cit. Rotation speed = 167.6 s^{-1}. Room temperature = 22°C.

One of the incentives for studying Cu-Ni alloy deposition is to be able to plate Monel alloy which typically contains 67% nickel, 30% copper, and the rest mostly iron and other elements. Although we have not plated 70/30 Ni-Cu alloy, we can predict the conditions necessary to produce such an alloy from the model. All the results indicate that the solution composition is an important variable in determining the deposit composition. A high nickel content deposit would require a solution containing high nickel. For instance, if we maintain as before the same plating temperature (22°C) and rotation speed (1600 rpm) and drop the copper content from 5 to 1%, then the model can be used to predict the deposit composition curve shown in Fig. 7. The curve demonstrates that, under the stated conditions, the deposition potential should be −1.08V *vs.* SCE. Various other combinations of operating conditions could be used to obtain a desired alloy composition.

The capability of the model demonstrated here is useful in designing and optimizing the Cu-Ni alloy electrodeposition process since there is only a narrow potential range for producing suitable deposits. Although the model presented in this report is limited to the rotating disk electrode, it can be extended to other geometric configurations such as the rotating cylinder or flow between parallel plates.

Conclusions

1. The model agreed well with the experimentally-obtained polarization curves, the alloy deposit composition, and current efficiency results.
2. Although the model does not consider the various effects of gas bubbles near the electrode, the inclusion of the kinetics of the hydrogen evolution reaction from the reduction of water in the model effectively predicted the loss in current efficiency.
3. Through data fitting, the model provides a means of estimating mass transport and kinetic parameters when multiple electrode reactions are occurring simultaneously.
4. The predictive capability of the model can be useful in designing and optimizing the alloy plating operation.
5. This model may be applied to other normal alloy deposition systems such as Bi-Cu, Pb-Sn, and Ag-Pd alloys. Only a few fundamental measurements specific to the system would be needed. It is recommended that the model is made to fit the behavior under one set of operating conditions and then tested against the behavior under another set of conditions for accuracy.

Manuscript submitted Dec. 14, 1987; revised manuscript received May 2, 1988. This was in part Paper 546 presented at the Atlanta, GA, Meeting of the Society, May 15-20, 1987.

General Motors Research Laboratories assisted in meeting the publication costs of this article.

LIST OF SYMBOLS

α	0.51023
a_k	activity of metallic species k
c_i	concentration of species i, mol/cm^3
$c_{i,ref}$	reference concentration of species i, mol/cm^3
$c_{i,\infty}$	bulk concentration of species i, mol/cm^3
$c_{i,o}$	concentration of species i adjacent to the surface, mol/cm^3
D_i	diffusion coefficient of species i, cm^2/s
D_R	diffusion coefficient of the diffusion controlling species, cm^2/s
E_{appl}	$V - \Phi_{RE}$, V
$\mathbf{F}$	Faraday's constant, 96,487 C/mol
i_j	current density due to reaction j, A/cm^2
$i_{oj,ref}$	exchange current density evaluated at reference concentrations for reaction j, A/cm^2
$i_{oj,data}$	exchange current density evaluated at data concentrations for reaction j, A/cm^2
n_j	number of electrons transferred in reaction j
N_i	flux vector of species i, mol/cm^2-s
p_{ij}	anodic reaction order of species i in reaction j
q_{ij}	cathodic reaction order of species i in reaction j
R	universal gas constant, 8.314 J/mol-K
R_i	homogeneous production reaction rate of species i, mol/cm^3-s
s_{ij}	stoichiometric coefficient of species i in reaction j
T	absolute temperature, K
$U_{j,ref}$	theoretical open-circuit potential evaluated at reference concentrations, V
$\mathbf{v}$	electrolyte velocity vector, cm/s
V	potential of the working electrode, V
y	normal coordinate, cm
z_i	charge number of species i

Greek symbols

α_{aj}	anodic transfer coefficient for reaction j
α_{cj}	cathodic transfer coefficient for reaction j
δ	diffusion layer thickness, cm
γ^{kj}	exponent in the composition dependence of exchange current density
ν	kinematic viscosity, cm^2/s
ξ	dimensionless distance
Φ	potential in solution within diffusion layer, V
Φ_o	solution potential adjacent to electrode surface, V
Φ_{RE}	potential in the bulk solution at $y = 3\delta$, V
ω	rotation speed of the disk electrode, s^{-1}
χ_k	mole fraction of metallic species k

APPENDIX

Calculation of Bulk Concentrations

For simplicity, let the concentrations be expressed in terms of X_i, and d_i

$X_1 = [CuCit^-]$, $X_2 = [CuHCit]$, $X_3 = [Cu^{2+}]$, $X_4 = [Cit^{3-}]$,

$X_5 = [HCit^{2-}]$, $X_6 = [H_2Cit^-]$, $X_7 = [H_3Cit]$, $X_8 = [NiCit^-]$,

$X_9 = [NiHCit]$, $X_{10} = [Ni^{2+}]$, $X_{11} = [SO_4^{2-}]$, $X_{12} = [HSO_4^-]$,

$X_{13} = [OH^-]$, $X_{14} = [H^+]$, $X_{15} = [Na^+]$,

$d_1 = [Cit^{3-}]_{total}$, $d_2 = [Cu^{2+}]_{total}$, $d_3 = [Ni^{2+}]_{total}$

$d_4 = [SO_4^{2-}]_{total}$.

The equilibrium constants for the reactions [1]-[9] can be expressed as follows

$$K_1 = \frac{X_1}{X_3 X_4} \quad [A\text{-}1]$$

$$K_2 = \frac{X_2}{X_3 X_5} \quad [A\text{-}2]$$

$$K_3 = \frac{X_{14} X_4}{X_5} \quad [A\text{-}3]$$

$$K_4 = \frac{X_{14} X_5}{X_6} \quad [A\text{-}4]$$

$$K_5 = \frac{X_{14} X_6}{X_7} \quad [A\text{-}5]$$

$$K_6 = \frac{X_8}{X_{10} X_4} \quad [A\text{-}6]$$

$$K_7 = \frac{X_9}{X_{10} X_5} \quad [A\text{-}7]$$

$$K_8 = \frac{X_{12}}{X_{11} X_{14}} \quad [A\text{-}8]$$

$$K_9 = X_{13} X_{14} \quad [A\text{-}9]$$

Thus, the material conservation equations (Eq. [10]-[13]) become

$$d_1 = X_1 + X_2 + X_4 + X_5 + X_6 + X_7 + X_8 + X_9 \quad [A\text{-}10]$$

$$d_2 = X_1 + X_2 + X_3 \quad [A\text{-}11]$$

$$d_3 = X_8 + X_9 + X_{10} \quad [A\text{-}12]$$

$$d_4 = X_{12} + X_{11} \quad [A\text{-}13]$$

and the electroneutrality condition is

$$\Sigma z_i X_i = 0 \quad [A\text{-}14]$$

Equations [A-1] through [A-14] provide an independent set of 14 nonlinear equations for the 14 unknowns ($X_1 - X_{14}$) in terms of the set values of $K_1 - K_9$, $d_1 - d_4$, and X_{15}. This set of equations can be simplified and solved.

The procedure to do this consists of setting a value for X_{14} and then rewriting Eq. [A-1] to [A-13] for X_4 in terms of X_{14}. The resulting equation is then solved iteratively for X_4, which then yields values for $X_1 - X_{13}$. In our case, X_{14} is a known value and is easily determined from pH measurement.

Substituting Eq. [A-3], [A-4], and [A-5] into Eq. [A-10] yields

$$d_1 = X_1 + X_2 + \alpha X_4 + X_8 + X_9 \quad [A\text{-}15]$$

where

$$\alpha = 1 + \frac{X_{14}}{K_3} + \frac{X_{14}^2}{K_3 K_4} + \frac{X_{14}^3}{K_3 K_4 K_5}$$

Substitution of Eq. [A-6] and [A-7] into Eq. [A-12] gives

$$X_8 + X_9 = \frac{X_4 \beta d_3}{\beta X_4 + 1} \quad [A\text{-}16]$$

where

$$\beta = K_6 + \frac{K_7 X_{14}}{K_3}$$

Combination of Eq. [A-1], [A-2], [A-3], [A-15], and [A-16] yields

$$d_1 = X_4 \left[e X_3 + \alpha + \frac{\beta d_3}{\beta X_4 + 1} \right] \quad [A\text{-}17]$$

where

$$e = K_1 + \frac{K_2}{K_3} X_{14}$$

From Eq. [A-1], [A-2], and [A-11], it is found that

$$d_2 = X_3 [1 + e X_4] \quad [A\text{-}18]$$

Combination of Eq. [A-17] and [A-18] gives

$$\left[e\beta \frac{d_2}{1 + e X_4} + \alpha\beta \right] X_4^2 + \left[e \frac{d_2}{1 + e X_4} + \alpha + \beta d_3 - d_1 \beta \right] X_4 - d_1 = 0 \quad [A\text{-}19]$$

From Eq. [A-19], it is obtained that

$$X_4 = \frac{-B + \sqrt{B^2 + 4Ad_1}}{2A} \qquad [A\text{-}20]$$

where

$$B = \frac{ed_2}{1 + eX_4} + \alpha + \beta d_3 - d_1\beta$$

$$A = \frac{e\beta d_2}{1 + eX_4} + \alpha\beta$$

Equation [A-20] is solved for X_4 by using an iterative method. That is, substitution of an initial guessed value of X_4 into the right-hand side of Eq. [A-20] gives a new value of X_4. Making use of this new X_4 as an initial value gives another new X_4. This process is repeated until the initial and new values of X_4 are equal to within a specified tolerance.

Once obtained, X_1, X_2, etc. can be obtained as follows

$$X_3 = \frac{d_2}{1 + \left(K_1 + \frac{K_2 X_{14}}{K_3}\right) X_4}$$

$$X_5 = \frac{X_{14}X_4}{K_3}$$

$$X_2 = K_2X_3X_5$$

$$X_1 = K_1X_3X_4$$

$$X_6 = \frac{X_{14}X_5}{K_4}$$

$$X_7 = \frac{X_{14}X_6}{K_4}$$

$$X_{10} = d_3\left[1 - \frac{K_8X_4 + K_7X_5}{K_6X_4 + K_7X_5 + 1}\right]$$

$$X_8 = K_6X_{10}X_4$$

$$X_9 = K_9X_{10}X_5$$

$$X_{11} = \frac{d_4}{K_8X_{14} + 1}$$

$$X_{12} = K_8X_{11}X_{14}$$

$$X_{13} = \frac{K_9}{X_{14}}$$

Once X_1 to X_{15} are determined, the electroneutrality condition is tested. Any residue is taken to represent some ionic species neglected in the summation. That is, let

$$z_{\text{pseudo}}\, c_{\text{pseudo}} = -\sum_{i=1}^{15} z_i X_i$$

This pseudo species can symbolize impurities in the deionized water, or other contaminants in the chemicals. When the pH is raised or lowered by the addition of an acid or base, the pseudo species includes the anions or cations associated with these additions.

REFERENCES

1. K. Vu Quang, E. Chassaing, B. Le Viet, J. P. Celis, and J. R. Roos, *Met. Finish.*, 25 (Oct. 1985).
2. A. Brenner, "Electrodeposition of Alloys, Principles, Practice," Vol. 1, pp. 558-584, Academic Press, Inc., New York (1963).
3. B. H. Priscott, *Trans. Inst. Met. Finish.*, **36,** 93 (1959).
4. J. R. Roos, J. P. Celis, C. Buellens, and D. Goris, *Proc. Metall.*, **3,** 177 (1984).
5. M. Ishikawa and H. Enomoto, *New Materials and New Processes*, **2,** 243 (1983).
6. R. Y. Ying, *This Journal*, **135,** 2957 (1988).
7. M. F. Mathias and T. W. Chapman, *ibid.*, **134,** 1408 (1987).
8. A. Ringbom, "Complexation in Analytical Chemistry," John Wiley & Sons, Inc., New York (1963).
9. N. A. Lange, "Lange's Handbook of Chemistry," 13th ed., McGraw Hill, Inc., New York (1985).
10. "CRC Handbook of Chemistry and Physics," 59th ed., R. C. Weast, Editor, CRC Press, Inc., Boca Raton, FL (1978-1979).
11. J. S. Newman, "Electrochemical Systems," Prentice-Hall, Inc., Englewood Cliffs, NJ (1973).
12. R. E. White, S. E. Lorimer, and R. Darby, *This Journal*, **124,** 1123 (1983).
13. A. J. Bard and L. R. Faulkner, "Electrochemical Methods: Fundamentals and Applications," John Wiley & Sons, Inc., New York (1980).
14. R. E. White, *Ind. Eng. Chem. Fund.*, **17,** 367 (1978).

Aqueous Solubilities, Solubility Products and Standard Oxidation-Reduction Potentials of the Metal Sulfides

Stuart Licht*

Department of Chemistry, Clark University, Worcester, Massachusetts 01610

ABSTRACT

Available thermodynamic data, incorporating a new free energy of formation for aqueous S^{2-} of 111 (±2) kJ/mol at 25°C, indicate that solubility products of the insoluble metal sulfide salts are several orders of magnitude smaller than previously considered. Thermodynamic characterization for a variety of soluble and insoluble aqueous metal sulfide systems is reported. Trends in the aqueous solubilities of the alkali salts solubilities are compared and discussed. New aqueous solubility products, K_{sp}, and standard redox potentials, $E°$, for over forty metal sulfides are determined. The new values of pK_{sp} and $E°$ at 25°C include: Ag_2S-orthorhombic: 53.6, −0.786V, and HgS-red: 56.4, −0.816V. Significant free S^{2-} occurs only in extremely alkaline media. The suitability of $\Delta G°_f(HS^-)$, rather than $\Delta G°_f(S^{2-})$, based solubility products and redox potentials is discussed and these alternate values determined.

Metal sulfides vary enormously in their solubility in water. At room temperature K_2S is soluble to approximately 50% by weight in water (1), whereas HgS is soluble to the equivalent of less than one atom of Hg per liter (2). This is reflected in the response of sulfide ion selective electrodes which display an effective potential response to sulfide (3) or metal cations (4) of 20 or more orders of magnitude. In practice, concentrations of metal are maintained in aqueous solutions containing even the highly insoluble metal sulfides, through formation and equilibrium interaction with metal hydrosulfide and metal sulfide complexes including $M_x(HS)_y$ in acidic environments and $(M_xS_y)^{z-}$ in alkaline environments.

* Electrochemical Society Active Member.